EurJIC
European Journal of Inorganic Chemistry

Research Article
doi.org/10.1002/ejic.202200374

Chemistry Europe
European Chemical Societies Publishing

www.eurjic.org

Bond Strength of a Diatomic Acceptor Ligand: A Reliable Measure of Its Antibond Occupation and Its Charge?

Jens Popp[a] and Peter Klüfers*[a]

Dedicated to Professor Wolfgang Beck on the occasion of his 90th birthday

A nitrosyl ligand is bonded to a central metal mainly via a mostly covalent normal bond and a coordinative metal-to-NO π-backbond. A recent analysis had unravelled similar bonding characteristics of both linear and bent CoNO moieties in terms of ligand charge and antibond occupation. Thus, there should be no justification for the usual assignment of an NO^+ ligand to a linear MNO unit and a singlet-NO^- ligand to a bent one. This claim seems to contradict that bending an MNO unit weakens the N–O bond with a marked red-shift of the N–O stretch as one indicator. In this work, the failure of Dewar-Chatt-Duncanson-derived conclusions is demonstrated for linear/bent isomer couples by the analysis of M–N and N–O bond strengths. Instead of DCD behavior, lateral electrostatic influence on NO and other diatomic ligands modulates the intraligand bond strength in a similar way as has been shown in former work for polar interaction of a charge with CO in the 'non-classical' carbonyls. Methodologically, local-mode analysis is used to determine bond strengths. Oxidation states are determined by the effective-oxidation-state (EOS) method.

Introduction

The Dewar-Chatt-Duncanson model (DCD model, Scheme 1), which describes the synergetic bonding of an electron-rich central metal atom and a donor/acceptor ligand, is a basic concept of coordination chemistry. A prototypical example that demonstrates the concept is provided by the series of carbonyliron complexes $[Fe(CO)_6]^{2+}$, $[Fe(CO)_5]$, and $[Fe(CO)_4]^{2-}$. Characterized by the shift from a Lewis-acidic, electron-poor low-spin-d^6-iron(II) to a Lewis-basic, electron-rich d^{10}-iron(−II) center, the metal's capability to form two Fe→CO backbonds in addition to an Fe←CO donor bond increases along the series. Scheme 1 points to appropriate methods to detect the extent of backbonding. Due to the concomitant decrease of the C–O bond order on increasing the weight of the right Lewis formula, the C–O distance increases, and the (typically well observable) C–O stretching vibration experiences a red-shift whereas the (rarely reported) M–C stretch is blue-shifted. The equivalent of the Lewis formulation in a molecular-orbital formalism is the increase of the occupation of the two C–O π* MOs on increasing weight of the metal-to-CO π-backbonds.

The DCD-typical countermovement of M–C-backbond and C–O-bond strengths in a series of related species may be quantified by the local modes of the M–C and C–O stretches as a reliable bond-strength measure.[2] For the series of the three prototypic iron carbonyls, Table 1 shows almost a duplication of the local stretching force constant k^a of the Fe–C bonds from Fe^{II} to Fe^{-II} when, at the same time, the C–O force constant is very roughly halved. In terms of carbonyl wavenumbers, the increasing extent of backbonding generates an approximately 200 cm^{-1} shift and more for each two-step change of the iron's oxidation state. (Note that normal and local modes are roughly the same in the highly symmetric species of Table 1 since the expected lowering of the local C–O mode by its decoupling from the Fe–C mode is balanced by the inclusion of the high-energetic but IR-forbidden $A_{1(g)}$ modes in the local-mode analysis. We will not find this effect in the mononitrosyls of this work; due to their lower symmetry no forbidden N–O modes occur.)

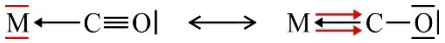

Scheme 1. The DCD model in its Lewis formulation (without formal charges). With *z* as the M–C–O axis, the metal contributes d(*xz*) and d(*yz*) lone pairs (red) to π-backbonds. The metal's acceptor orbital for the σ-donor bond from CO is, for a 3d metal, of mostly $3d_{z^2}$ character if empty; if $3d_{z^2}$ is occupied by metal electrons, empty 4s/4p orbitals admix to accept the carbon lone pair. In agreement with the typical thermal decomposition of an MCO moiety to M and CO all M–CO bonds are coordinative bonds.[1]

Notably, due to the almost constant charge drain from the ligands through the Fe←CO donor bonds (see the last column of Table 1 and the explanations below), increasing backbonding goes along with an increasing negative charge of the acceptor ligands as a result of the increasing occupation of the C–O-π* orbitals (Q_{CO} column in Table 1).

Nitrosyl complexes generally fit into this conceptual framework, as do cyanido complexes. Table 1 and Table 2 show the values of both the carbonyl and the nitrosyl ligands in the mixed-ligand d^{10}-Fe^{-II} species $[Fe(CO)_3(NO)]^-$, which is a {FeNO}^{10}

[a] J. Popp, Prof. Dr. P. Klüfers
Department Chemie
Ludwig-Maximilians-Universität München
Butenandtstraße 5–13, 81377 München, Germany
E-mail: kluef@cup.uni-muenchen.de
https://www.cup.lmu.de/ac/kluefers/homepage

Supporting information for this article is available on the WWW under https://doi.org/10.1002/ejic.202200374

Research Article
doi.org/10.1002/ejic.202200374

Chemistry Europe
European Chemical Societies Publishing

Table 1. BP86/def2-TZVP-computed values of carbonylmetal species. The $\tilde{\nu}_{IR}$ column lists the IR-allowed C–O stretches (see Table S4 in the Supporting Information for the experimental values). For the three homoleptic carbonyls, IR-forbidden, totally symmetric stretches at higher excitation energy contribute to the local modes. Q_{CO} is the QTAIM (Quantum Theory of Atoms In Molecules) charge of the carbonyl ligand, k^a and $\tilde{\nu}^a$ are the local force constants of the M–C and C–O bonds and the equivalent local wavenumber of the C–O stretch. λ values (in electron pairs) are Topological Fuzzy Voronoi Cell (TFVC) gross occupations of the π-antibonding effective fragment orbitals (EFOs) and the EFO of the σ-donor pair (largely the canonical CO-3σ MO). For an extended version of the table see Table S8 in the SI (C–O distances, TFVC gross and Mulliken charges).

	$\tilde{\nu}_{IR}$/cm^{-1}	Q_{CO}/e	$k^a_{M\text{-}C}$/N cm^{-1}	$k^a_{C\text{-}O}$/N cm^{-1}	$\tilde{\nu}^a$/cm^{-1}	$\lambda_{\pi^*(CO)}$	$\lambda'_{\pi^*(CO)}$	$\lambda_{\sigma\text{-donor}}$
$[Fe(CO)_6]^{2+}$	2168	0.17	1.89	19.06	2172		2×0.08	0.75
$[Fe(CO)_5]$	1988, 1956	−0.16	2.79	15.76	1975		2×0.17	0.75
$[Fe(CO)_4]^{2-}$	1704	−0.66	3.33	11.62	1696		2×0.24	0.77
$[Fe(CO)_3(NO)]^-$	1948, 1837	−0.40	3.04	13.68	1840		2×0.20	0.77
$[Co(CO)_3(NO)]$	2064, 1977	−0.09	2.47	15.85	1980		2×0.14	0.78

Table 2. BP86/def2-TZVP-computed values of nitrosylmetal species. QTAIM charges Q of the nitrosyl ligand, local force constants k^a of the M–N and N–O bonds including the equivalent local wavenumber $\tilde{\nu}^a$ of the N–O stretch, and TFVC gross occupation λ (in electron pairs) of the π-antibonding EFOs and the EFO of the σ-donor pair (the canonical NO-3σ MO which largely resembles the lone pair at N in the Lewis formulae). The normal modes of $[Fe(CO)_3(NO)]^-$ and $[Co(CO)_3(NO)]$ are practically free of carbonyl admixtures but contain about 10–15 % M–N coupling. For an extended version of the Table see Table S9 in the SI (TFVC gross and Mulliken charges, contribution of the three MOs of the last columns to the total charge of the nitrosyl ligand).

	MNO/°	$\tilde{\nu}_{NO}$/cm^{-1}	$d_{N\text{-}O}$/Å	Q_{NO}/e	$k^a_{M\text{-}N}$/N cm^{-1}	$k^a_{N\text{-}O}$/N cm^{-1}	$\tilde{\nu}^a_{NO}$/cm^{-1}	$\lambda_{\pi^*(NO)}$	$\lambda'_{\pi^*(NO)}$	$\lambda_{\sigma\text{-donor}}$
$[Fe(CO)_3(NO)]^-$	180	1628	1.196	−0.61	5.00	10.54	1548		2×0.43	0.84
$[Co(CO)_3(NO)]$	180	1802	1.160	−0.25	4.63	13.37	1743		2×0.35	0.85
1 (*TBPY*-5, GS)	180	1794	1.161	−0.24	4.38	13.13	1727	0.42	0.28	0.85
1′ (*SPY*-5)	157	1759	1.162	−0.23	3.47	12.61	1693	0.35	0.31	0.87
1′Cl (*SPY*-5 + 1)	126	1558	1.193	−0.38	2.11	10.34	1533	0.48	0.23	0.91
2′ (*TBPY*-5)	177	1824	1.163	−0.24	4.24	13.59	1757	0.45	0.24	0.84
2 (*SPY*-5 + 1, GS)	123	1637	1.185	−0.27	2.37	11.37	1607	0.45	0.21	0.92
3′ (*TBPY*-5)	162	1751	1.169	−0.29	3.65	12.04	1654	0.45	0.26	0.85
3 (*SPY*-5, GS)	141	1666	1.177	−0.28	2.92	11.51	1617	0.40	0.28	0.90
$[Fe(CN)_5(NO)]^{2-}$ (GS)	180	1893	1.145	−0.07	4.77	14.88	1839		2×0.32[a]	0.84[a]
$[Fe(CN)_5(NO)]^{2-}$ (MS2)	82	1595	1.182	−0.10	2.07[b]	10.20	1523	0.42	0.19	0.99[c]
$[RuCl_2(his)(NO)]$ (GS)	175	1845	1.158	−0.20	5.55	13.63	1760	0.38	0.37	0.82
$[RuCl_2(his)(NO)]$ (MS2)	88	1499	1.207	−0.27	2.97[d]	9.07	1436	0.45	0.27	0.97[e]

[a] *trans*-cyanido ligand for comparison: $Q/e = -0.58$, $\lambda = 2\times0.05$, 0.69. [b] Accompanied by k^a/N cm^{-1} = 1.07 for the Fe–O contact in this side-on coordination. [c] N–O π-bond instead of 3σ as a M←XY donor: $\lambda = 0.91$. [d] Accompanied by k^a/N cm^{-1} = 0.89 for the Ru–O contact in this side-on coordination. [e] N–O π-bond instead of 3σ as a M←XY donor: $\lambda = 0.90$.

species in the nitrosyl-specific Enemark-Feltham nomenclature (there, the superscript gives the number of metal-d electrons if NO^+ is assumed as the ligand).[3] In the ferrate, the parameters of the FeCO moieties mirror the enhanced π-acidity of the stronger accepting NO^+ competitor ligand by decreased back-bonding from the central metal compared to the isoelectronic d^{10}-Fe^{-II} $[Fe(CO)_4]^{2-}$ species. The parameters of the nitrosyl ligand mirror its stronger π-acidity. The Fe–N local force constant reaches a maximum, and the lowest force constant among the diatomic ligands discussed until now is reached. The inclusion of another isoelectronic species, $[Co(CO)_3(NO)]$, with a lower overall charge and, thus, lower electron density at the metal center and lower backbonding capability, shows all the trends for the parameters of both ligand types (Table 1 and Table 2) which are expected for a DCD system.

The individual contributions of σ-donation and π-acceptance of the diatomic ligand are given in the last three columns of Table 1 and Table 2. The tabulated numbers are occupations of 'effective fragment orbitals' (EFOs) which have been introduced in the framework of computational oxidation-state (OS) determination.[4] In this approach, the tabulated EFOs show the partitioning of the electron pairs between their bonding partners (Figure S1 in the SI illustrates the principle of an EFO partitioning). Table 1 and Table 2 show the occupations of the three ligand orbitals of the DCD scheme, the, prior to metal-bonding, filled σ-donor and the two empty π*-acceptor MOs. For the carbonyls (Table 1), about 3/4 of the donor pair remains allocated at the ligand, whereas a maximum of about 1/4 pair is transferred from the filled metal d-orbitals to each of the C–O π* antibonds via backbonds. These numbers give a rationale for the determination of OSs. In the heterolytic cleavage procedure of an OS assignment, the backbonds go to the metal and the donor bond falls to the ligand.

The EFOs mirror the characteristics of the isoelectronic ligands CN^- and NO^+. *The* prototypic nitrosyl complex nitroprusside, $[Fe(CN)_5(NO)]^{2-}$, contains both ligands. With an occupation of 0.69 electron pairs, the *trans*-cyanide's donor pair has lost more electron density than a CO ligand of a carbonyl, while the minor occupation of the cyanide's antibonds with 2× 0.05 electron pairs shows the almost pure donor character of a cyanido ligand (0.70 and 2×0.06 for the four *cis*-cyanides). The opposite holds for nitroprusside's nitrosyl ligand (Table 2). Its donor pair donates little electron density to iron ($\lambda = 0.84$) but backbonds fill the N–O antibonds with 2×0.32 electron pairs. The carbonyls of Table 1 lie in between the cyanide/nitrosyl values. However, in all these cases, the π-bonding electron pairs remain concentrated at the metal (and thus go to the metal on OS assignment; see Table S7 in the SI).

Research Article
doi.org/10.1002/ejic.202200374

Notably, donation by a given ligand's lone pair is a virtual constant. In agreement with this finding, published practice often follows a simplified procedure to assess the diatomic ligand's charge. Due to (1) the usually excellent observability of the diatomic's stretch, (2) the often lacking assignment of the M–N stretch, (3) the constant charge depletion through the donor bonds, and (4) a sufficient correlation of normal and local vibrational modes, a red-shift of the diatomic ligand's valence stretch appears to unbiasedly mirror the occupation of the ligand's antibonds and its charge.

This simplified procedure to deduce the charge of a nitrosyl ligand from its N–O stretch has caused far-reaching conclusions in the case of bent MNO moieties which are predominant for $\{MNO\}^8$ species.[5] Specifically, the marked red-shift on transforming a linear to a bent $\{MNO\}^8$ moiety seems to support the assignment of an NO^+ ligand to the former and an NO^- ligand to the latter. Scheme 2 highlights these assignments of an $\{MNO\}^8$ species which forms, in its *TBPY*-5-type linear isomer with NO in the equatorial plane, non-degenerate π-bonds (see below).

Attempts to rationalize this 'traditional' view at OSs computationally for the $\{CoNO\}^8$ subclass, however, left us, on the one hand, with the result that no significant difference between the linear and bent species can be detected in terms of ligand charge and antibond occupation.[5] On the other hand, the red-shift on bending is obvious (as is a somewhat larger N–O distance in the bent class). Thus, which method provides us with the decisive numbers? Is there an inconsistency between IR spectroscopy and X-ray analyses on the one hand and population analyses on the other? (For an anonymous referee of Ref.[5] the decision was clear: "… the N–O stretch between compounds of the bent and linear type differs by 130–150 cm^{-1} (or more), which demonstrates, experimentally!, that there is a noticeable difference in the occupation of the π* orbitals of the NO ligand between the bent and the linear structures.") With this work, we wish to show that the correlation between a diatomic ligand's valence stretch and its charge is lost if the DCD model loses its applicability – as it does in a linear/bent transformation.

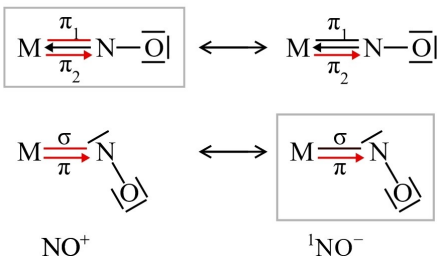

Scheme 2. Lewis formulae (without formal charges) of linear and bent $\{MNO\}^8$ groups comprising all valence electrons of NO (black) and two metal pairs (red). The more covalent, in Haaland's sense normal, M–NO bond (the one to which $\lambda_{\pi^*(N\text{-}O)}$ is assigned in Table 2) which is assumed to be the homolytically cleaved one on dissociation to M and NO, decides on oxidation-state assignment.[1] If assigned to the metal, an $M^n(NO^+)$ couple results, if assigned to the ligand, the result is $M^{n+2}(NO^-)$. The grey-framed formulae highlight the customary choice. Contrarily, oxidation-state assignment by the EOS method results in $M^n(NO^+)$ for all species of Table 2 including the bent ones (Table S7 in the SI).

Results and Discussion

A linear $\{MNO\}^8$ ground state

We start our survey with a compound that allows us to include a retrospective look at the whole issue. It is a representative of the rarer case of a linear $\{MNO\}^8$ species, namely the new salt $[Co(dppe)_2(NO)](BF_4)_2 \cdot 2Me_2CO$ of the known $[Co(dppe)_2(NO)]^{2+}$ ion **1**, dppe = 1,2-bis(diphenylphosphino)ethane. Figure 1 (left) shows the molecular structure of **1** which is the only second example of a well resolved crystal-structure analysis of a linear $\{CoNO\}^8$ moiety. Moreover, **1** is an analogue of the historically important species $[Co(das)_2(NO)]^{2+}$ [das = 1,2-bis(dimethylarsino)benzene], the perchlorate of which was published more than half a century ago by Feltham.[6] In terms of DCD-

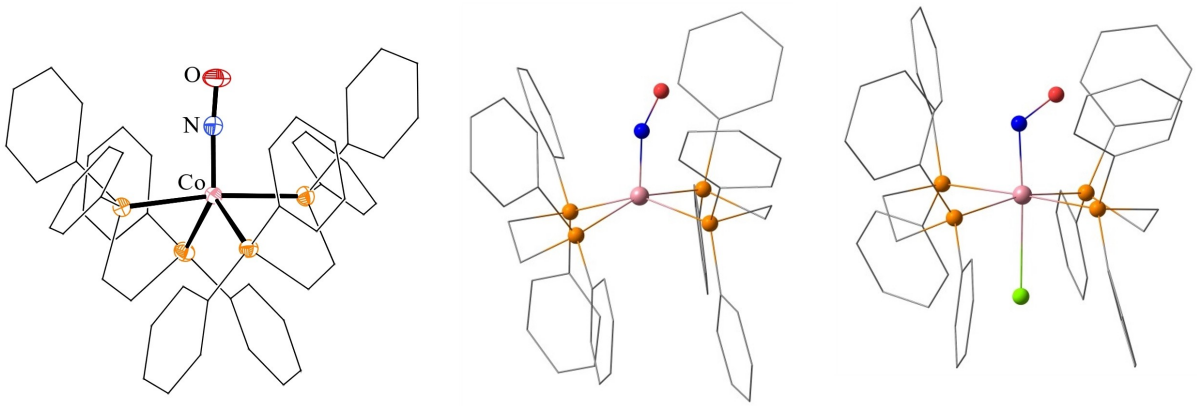

Figure 1. Left: the *TBPY*-5-configured cation **1** in crystals of $[Co(dppe)_2(NO)](BF_4)_2 \cdot 2Me_2CO$, 50% ellipsoids for the heavier atoms; $\tilde{\nu}_{exp} = 1814\ cm^{-1}$; distances in Å and angles in °: Co–N 1.662(2), N–O 1.157(3), Co–N–O 173.7(2); calc.: Co–N 1.661, N–O 1.161, Co–N–O 179.7. **Middle**: a local minimum structure **1′** of the *SPY*-5 type, 24.4 kJ mol^{-1} above **1**; Co–N 1.687, N–O 1.162, Co–N–O 156.7. **Right**: Feltham's 'stereochemical control of valence', exemplified by the chlorido adduct **1′**Cl, an analogue of Feltham's bis(diarsane) derivative; Co–N 1.784, N–O 1.193, Co–N–O 126.2.

Research Article
doi.org/10.1002/ejic.202200374

related parameters, the {CoNO}^{8} species **1** (as well as Feltham's das analogue) is close to the {CoNO}^{10} species [Co(CO)$_3$(NO)], the larger electron number of the latter being counterbalanced by the electron-withdrawing carbonyl co-ligands (Table 2).

IR analysis of the das salt and (pseudo)halogenido adducts thereof led Feltham to formulate the concept of 'stereochemical control of valence' which he published, then together with Enemark, in a series of five papers on this topic.[7] In their influential 1974 review, there is a chapter on this concept as well.[3] Its essence may be exemplified by the chloride derivative: if chloride was added to the parent [Co(das)$_2$(NO)]$^{2+}$ species, Feltham found the N–O stretch red-shifted from 1852 cm^{-1} by about 300 cm^{-1} into a spectral region where typically N=O double bonds were found. Thus, he formulated (N=O)$^-$ as the ligand. A decade later, the same authors demonstrated by X-ray analysis that the nitrosyl ligand of the parent species was linearly bonded whereas the red-shift went along with a bent CoNO group *trans* to the entered chlorido co-ligand.[7d] Since then, the distinct red-shift of an MNO group on bending contributes a strong argument to the above-mentioned NO$^+$/NO$^-$ assignment. By the way, the free species NO$^+$ (2345 cm^{-1}), NO (1876 cm^{-1}) and NO$^-$ (1370 cm^{-1}) experience an about 500 cm^{-1} red-shift per one-electron reduction.[8]

The 'stereochemical control of valence' in Feltham's sense as a co-ligand's ability to perform a valence switch is illustrated in Figure 1 in terms of a computational approach starting with the experimental structure of **1**. Just as [Co(das)$_2$(NO)]$^{2+}$, **1** is a trigonal bipyramidal coordination entity with the nitrosyl ligand in an equatorial position. Addition of a chlorido ligand resulted, in our computer experiment, in the bending of the CoNO group from 180° to 126° (Figure 1, right; Table 2). In Feltham's sense, a Co$^{\rm I}$(NO$^+$) moiety changes its valences to Co$^{\rm III}$(^{1}NO$^-$) while, also here, a marked computed red-shift in the 200–300 cm^{-1} range is obtained. However, as observed for linear and bent {CoNO}^{8} systems with a larger number of various co-ligands, the red-shift on bending is not accompanied by a considerable increase of electron density on the nitrosyl ligand (Table 2).[5] In fact, a look at the DCD-related parameters shows that bending an MNO function is a non-DCD event.

The entries of **1** and **1′**Cl show the non-DCD-type characteristics of the linear-to-bent transformation: the computed red-shift is 236 cm^{-1}, which decreases to 194 cm^{-1} in terms of local modes (due to the more pronounced coupling of the Co–N and the N–O vibration in the linear case). Accordingly, the local force constant shows a decrease of the N–O bond strength on bending. However, contrary to DCD behavior, also the Co–N bond strength decreases on bending. Hence, bending softens both bonds, the M–N as well as the N–O bond. In fact, it is the Co–N bond which is more severely affected by the bend by halving its strength. Electron-density shifts seem to be of minor importance. However, to obtain a clear-cut picture, we examined a linear/bent transformation by a look at two true isomers with a zero charge balance.

A bent {MNO}^{8} ground state

As a starting point, Figure 2 shows a second new {CoNO}^{8} species, [Co(*N*,*N*-dmen)$_2$(NO)](ClO$_4$)$_2$ with the dication **2** (dmen = *N*,*N*-dimethylethylenediamine). As for the majority of {CoNO}^{8} compounds, the CoNO group is bent here. As a bis(ethylenediamine) derivative, **2** shares some properties with related dicationic species including the bis(en) parent ion, such as the somewhat distant bonding of a counterion (which is analyzed in more depth in Ref. [5]). An OS determination by the effective-oxidation-state method shows that also **2** is a Co$^{\rm I}$(NO$^+$) complex in terms of closed-shell singlet wavefunctions (Table S7 in the SI; see the Appendix for a discussion of methods which impose some diradicaloid character of **2**), the appropriate Lewis formulation of which is the bottom left formula of Scheme 2. Linearizing the CoNO function in a computational approach makes the *SPY*-5(+1)-configured [Co(*N*,*N*-dmen)$_2$(NO)](ClO$_4$)$^+$ entity jump into a local *TBPY*-5 minimum which resembles the ground-state structure of the bis(diphosphane) species **1** (Figure 2, right).

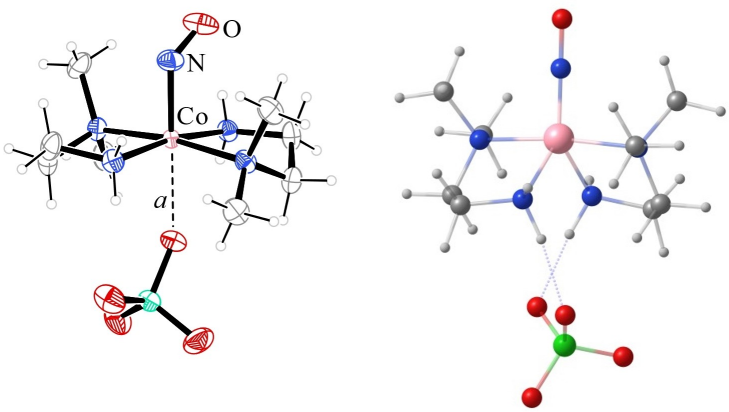

Figure 2. Left: the [Co(*N*,*N*-dmen)$_2$(NO)]$^{2+}$ cation **2** with the closer perchlorate counterion in crystals of the solvent-free bis-perchlorate, 50% ellipsoids; $\tilde{\nu}_{\rm exp}$ = 1655 cm^{-1}; distances in Å and angles in °: Co–N 1.809(2), N–O 1.165(2), Co–N–O 123.6(2), *a* = 2.394(2); calc.: Co–N 1.779, N–O 1.185, Co–N–O 122.9; *a* = 2.373. **Right**: a computed CoNO-linear isomer **2′**, 27.6 kJ mol^{-1} above the ground state **2**ClO$_4$; Co–N 1.650, N–O 1.163, Co–N–O 177.3.

Research Article
doi.org/10.1002/ejic.202200374

The results are collected in Table 2. Viewed from the local 180° to the global 126° minimum, bending results in an overall stabilization, total (187 cm^{-1}) and local (150 cm^{-1}) N–O red-shifts, only marginal changes of the nitrosyl charge and antibond occupation, and a pronounced softening of both the Co–N and the N–O bonds in terms of local force constants. Again, we see the clear non-DCD behavior of the transition.

Intermediate MNO angles

Before we try to tackle the physics behind these results, a widespread phenomenon of MNO chemistry will now be included: the variability of the MNO angle – with a focus on its IR-spectroscopic trace. The clear assignment of an $\{MNO\}^8$ species as linear or bent which we found in **2** and **2′** is not evident *per se*. An instructive example of angle variability was obtained on attempts to prepare the computed chlorido adduct to **1**. In the real-world experiment one of the diphosphane chelators of **1** was cleaved off on chloride addition and the new compound $[CoCl_2(dppe)(NO)]$ (**3**) was crystallized. Figure 3 (left) shows its molecular structure with a bend of 138° which is less pronounced than that in **1′**Cl and **2**. Also for **3**, the computational search for a more linear isomer succeeded. Figure 3 (right) shows the local minimum structure with a 165° bend of the CoNO function (**3′**). At this point it makes sense to also introduce a bent isomer of **1** which was computed by skipping off the chloride of **1′**Cl and allowing the structure to relax. The result is an isomer with a 157° bend (Figure 1, middle). It becomes clear that 'linear' and 'bent' are useful categories in clear cases, but ambiguity seems to arise if we try to distinguish between a 165° 'linear' isomer (**3′**) and a 157° 'bent' structure (**1′**).

However, all the isomers can be clearly assigned if, instead of the MNO angle, the coordination polyhedron about the metal is used as the classification criterion. Hence, both the clearly linear as well as the related borderline cases are of the *TBPY*-5 type, whereas both the clearly bent as well as the related borderline cases are of the *SPY*-5 type. Thus, the classification of $\{CoNO\}^8$ species in the sense of various types of 5-coordination (or 5 + 1) takes the focus away from the nitrosyl ligand. It's the metal's trade to arrange the NO ligand 'bent' (by donation of its d_{z^2} pair) or 'linearly' (by donation of its d_{xz} pair, see Ref.[5] for details). Moreover, the differences of the wavenumbers of the various N–O stretches (as well as the various local force constants) are clearly correlated with the angle difference within an isomer couple, not with the charge or the π* occupation of the nitrosyl ligand (Table 2). Finally, in agreement with this result, local force constants unravel the non-DCD behavior of the bent/linear couples. A bent-bonded nitrosyl ligand in an *SPY*-5 isomer shows a weaker N–O bond, but not via enhanced π* occupation.

Lateral charge–ligand interaction

However, what is the origin of the red-shift? The key to explain this phenomenon is provided by two publications that were, two and a half decades ago, devoted to the IR-spectroscopic characteristics of electron-poor ('non-classical') carbonyls such as the $[Fe(CO)_6]^{2+}$ species of Table 1.[9] The authors demonstrate that a positive unit charge Q^+ in linear QCO^+ bonding strengthens the C–O bond but weakens it in linear COQ^+ bonding. The result was further rationalized a decade ago into still more depth in terms of the effective electronegativity of an atom in the vicinity of a charge.[10]

In an extension of these approaches, we examined lateral interaction of a positive unit charge to a diatomic ligand XY. To include the metal positions of interest, we scanned a Q–X–Y angle range from 180° to 70° with the positive elementary charge at relaxed distance to XY (which refined close to 1 Å for all angles). Figure 4 shows the result for CO. The energy (blue crosses) is a minimum for the linear QCO^+ starting point and increases continually to the 70° side-on end point. Along this path, the C–O stretch experiences an about 400 cm^{-1} red-shift. In a step towards nitrosyl groups, the 'real' charge of a nitrosyl

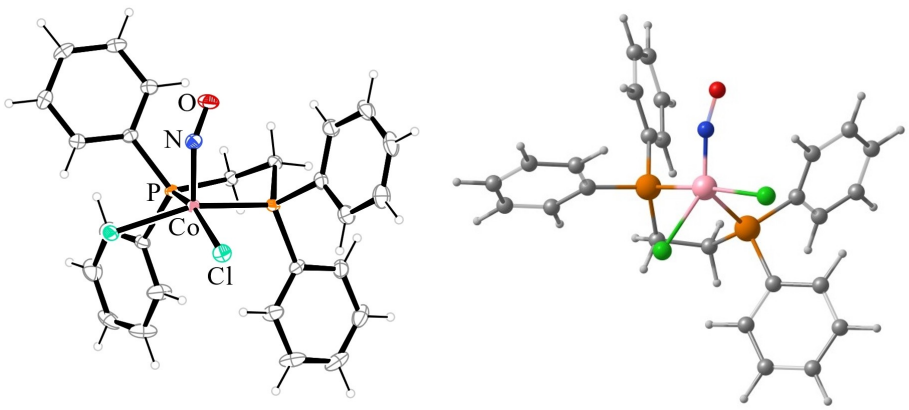

Figure 3. Left: coordination entities **3** in crystals of $[CoCl_2(dppe)(NO)]\cdot$acetone (**3**), 50% ellipsoids; $\tilde{\nu}_{exp} = 1667\ cm^{-1}$ (in acetone). Distances in Å and angles in °: Co–N 1.7498(13), N–O 1.173(2); Co–N–O 137.93(12); calc.: Co–N 1.719, N–O 1.177, Co–N–O 140.9. **Right**: the computed *TBPY*-5 'linear' isomer **3′**, 18.4 $kJ\,mol^{-1}$ above **3**; Co–N 1.660, N–O 1.169, Co–N–O 164.5.

Research Article
doi.org/10.1002/ejic.202200374

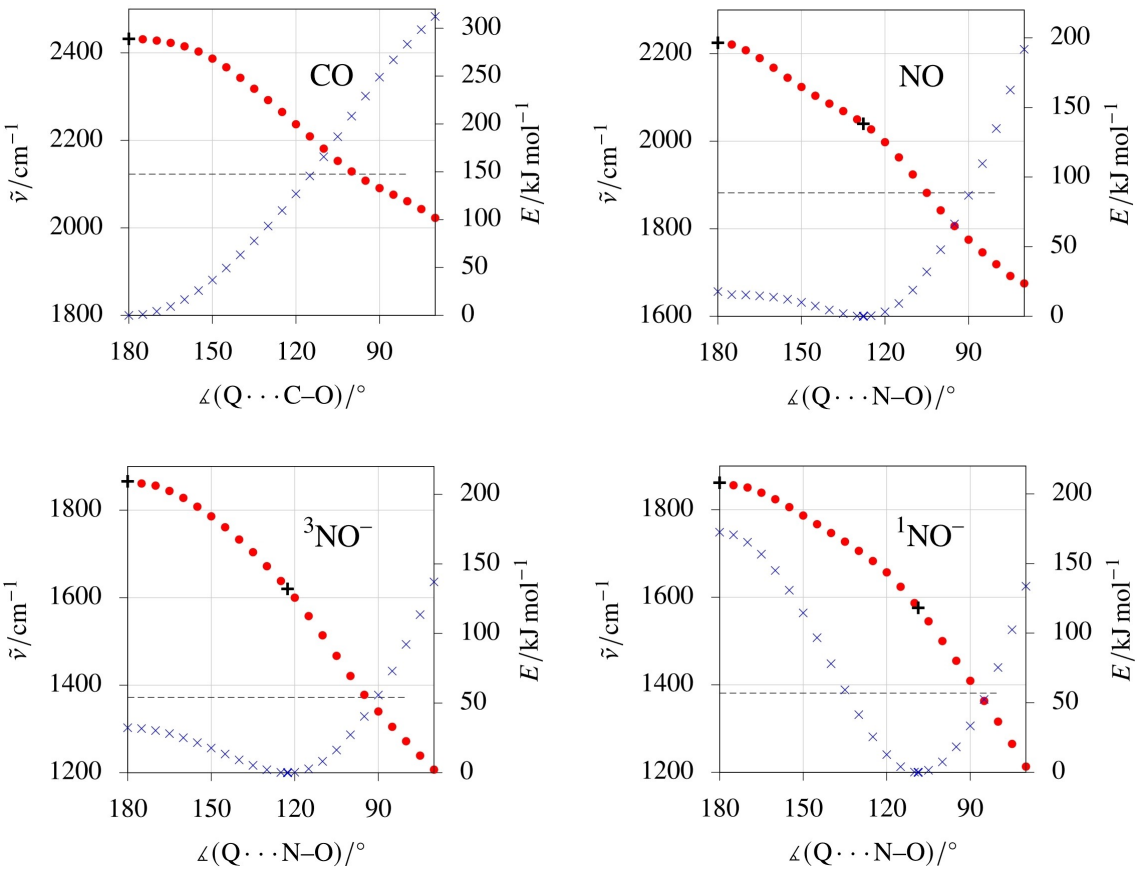

Figure 4. BP86/def2-TZVP-calculated stretching vibration $\tilde{\nu}$ (left axes, red dots) and relative energy (right axes, blue crosses) of diatomic species XY with a positive elementary charge Q^+ at angles Q···X–Y between 180° and 70°. Stationary points which were refined without the angle constraint are marked as black crosses. The dashed lines parallel to the abscissa marks the computed X–Y valence stretch in the absence of a charge ($\tilde{\nu}$/cm^{-1} for CO, NO, ^{3}NO$^-$, ^{1}NO$^-$: 2125, 1882, 1372, 1381, respectively); experimental values for CO, NO, ^{3}NO$^-$: 2143, 1876, 1370.[8]

ligand was used as a guideline. With typical QTAIM values of about −0.2 to −0.5 *e*, the inclusion of NO and the NO$^-$ forms seems appropriate. The result differs from CO in terms of stability. The NO species are stabilized in the vicinity of a Q–N–O angle of roughly 120°: NO and ^{3}NO$^-$ in a flat minimum, ^{1}NO$^-$ in a clear minimum (thus providing two stationary points along the paths; see the black crosses in Figure 4; in addition, see Figure S2 in the SI which provides data on a scan along fully relaxed stationary points). However, much more important for our problem is the trend of the N–O stretch's wavenumber. First, it is roughly the same for all electronic states – hence, conversely, our initial choice is of little influence on the result. Second, polar-to-lateral electrostatic modulation of the nitrosyl by a probe charge makes the vibration become soft by about 600–700 cm^{-1}.

A bent {MNO}^{6} excited state

To broaden these findings over the narrower context of {CoNO}^{8} species, the more extreme, but well established photo-induced linkage isomerism (PLI) will now be included. Here, metastable side-on linkage isomers of mostly {MNO}^{6} nitrosyls are experimentally accessible (often termed MS2 to distinguish these κ^2*N,O*-bonded states from metastable, κ*O*-bonded linear isonitrosyls, the MS1 states, and the κ*N*-bonded linear ground state, GS).[11] The sodium salt dihydrate of the above-mentioned nitroprusside, $Na_2[Fe(CN)_5(NO)]\cdot 2H_2O$ ('SNP'), was the first compound where these isomers had been detected and characterized.[12] (Note the more complicated case of multiplicity change on excitation as reported for $[Co(CO)_3(NO)]$.[13]) Here, we include the MS2 state of a {RuNO}^{6} species, $[RuCl_2(his)(NO)]$ (his = L-histidinate), which was detected IR-spectroscopically after irradiation of the linear ground state with green light.[14] Figure 5 shows the computed local minimum structure of the MS2 isomer, the N–O stretch of which was found more than 350 cm^{-1} red-shifted (Table 2 and caption to Figure 5). The latter value is typical for a GS/MS2 couple (compare the computed and experimental nitroprusside red-shifts of 298 cm^{-1} and 296 cm^{-1}, respectively).[12a] Moreover, Table 2 shows the typical non-DCD pattern of the relevant parameters. Still more pronounced than the bending of a {CoNO}^{8} species, the GS-to-MS2 transition heavily weakens the N–O bond without charging the nitrosyl ligand significantly.

To this end, we find a pronounced red-shift of several hundred reciprocal centimeters on lateral interaction of a

Research Article
doi.org/10.1002/ejic.202200374

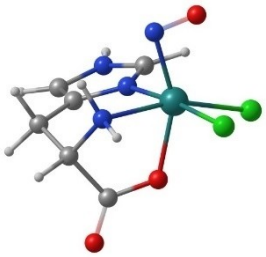

Figure 5. BP86/def2-TZVP-computed structure of the IR-spectroscopically detected MS2 isomer of [$RuCl_2$(his)(NO)], his = L-histidinate; 107.9 kJ mol^{-1} above the ground state; Ru–N–O: 88°; $\tilde{\nu}_{NO}$(exp) = 1537 cm^{-1}, compare $\tilde{\nu}_{NO}$(exp) = 1900 cm^{-1} for the linear GS. Table 2 contains the respective computed values.

positive charge with a nitrosyl moiety. Replacing the probe charge by a real metal fragment seems to maintain this correlation. As a result, bent isomers show markedly weakened N–O bonds in terms of the ligand's valence stretch or its atomic distances while local-mode analysis shows non-DCD behavior. Specifically, no significant increase of negative charge or π* antibond occupation is observed.

Other diatomic ligands

Plots such as those of Figure 4 are obtained with other diatomic ligands such as cyanide, peroxide or diazenide as well. Figure S3 in the SI shows the respective curves for a singlet-diazenide ion which is a current focus of research on nitrogen activation. In fact, the properties of coordinating dinitrogen species appear to be modulated on lateral bonding of either transition metal or alkali ions.[15] Similar observations have been made for peroxido ligands with laterally attached alkali ions in terms of O–O distances.[16] The key to this work came from carbonyl chemistry.[9] Also with this classical ligand, current controversies appear to be touched by our topic. As an example, the origin of the red-shift of the C–O stretch in alkaline-earth octacarbonyls is seen as a result of backbonding by the one group, or as a result of lateral CO···CO interactions by the other.[17] Moreover, new orbital-based concepts in carbonyl and cyanide chemistry such as 'side donation' might be inspected with respect to electrostatic aspects.[18]

Bond strength measures

In our study as well as in these related fields, atomic distances appear to be correlated with other bond-strength measures. Figure S4 in the SI shows, as a well-working example, the connection of the C–O bond length d and the local C–O force constant k^a of the five entries of Table 1 via a simple $k = A\ (d–B)^{-3}$ relationship, the so-called Badger's rule.[19] The virtually perfect correlation of Figure S4 is not attained for the nitrosyl ligand of the species of Table 2 (Figure 6, left). The larger spread of the data points appears to mirror the more complicated relationship of the force constant and the atomic distance as unraveled by the angle scan. The Q^+···N–O scan of Figure 6 (right) is typical. For small angles, Badger's rule holds. However, coming closer to linearity, the increase of the force constant goes along with a diminished decrease of the N–O distance.

Conclusion

We have shown how DCD-derived rules lose their applicability in non-DCD events such as bending the nitrosyl ligands of {MNO}^{8} and {MNO}^{6} species. These non-DCD (and non-Badger) transitions show the necessity to extend the electrostatic arguments which have been formulated to understand the spectroscopic peculiarities of non-classical carbonyl

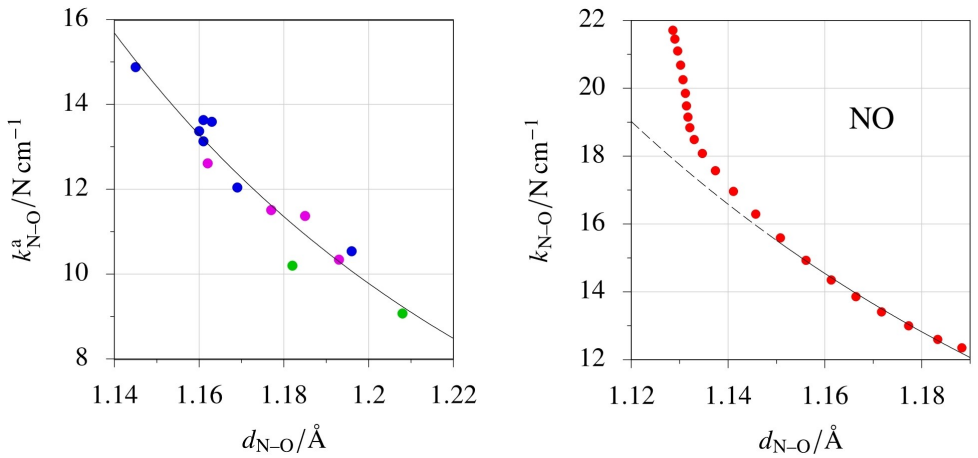

Figure 6. The $k = A\ (d–B)^{-3}$ relationship ("Badger's rule") with the force constant k, the atomic distance d and two adaptable parameters A and B.[19] **Left**: local force constant k^a_{N-O} vs. d_{N-O} for the nitrosyls of Table 2. The line shows a fit according to k^a/N cm^{-1} = 0.684 × (d/Å–0.788)$^{-3}$. Blue dots: linear MNO functions or *TBPY*-5 species; purple dots: *SPY*-5 species; green dots: MS2 species. **Right**: a Badger plot for the Q^+···N–O scan of nitric oxide (180 to 70° from left to right). The local force constant of a diatomic coincides with the standard force constant $k = \tilde{\nu}^2\ c^2\ 4\pi^2\ \mu$ with the speed of light c and the reduced mass μ. The Badger relationship k/N cm^{-1} = 1.481 × (d/Å–0.693)$^{-3}$ fits to those data points that are connected by the solid part of the line.

Research Article
doi.org/10.1002/ejic.202200374

complexes.[9–10] In particular, there is no justification to derive a diatomic ligand's charge and antibond occupation from bond-strength measures such as the ligand's valence vibration or the atomic distances. This result may be interesting for the area of small-molecule activation.[20] Bond weakening as an early step of bond cleavage in a small molecule's activation might or might not be accompanied by the transfer of charge in oxidation or reduction steps. Or, to formulate an answer to the title question "[is] a diatomic acceptor ligand's bond strength a reliable measure of its antibond occupation and its charge?": yes, for DCD, no, for non-DCD scenarios.

Experimental Section

Synthesis

Bis(1,2-bis(diphenylphosphino)ethane)nitrosylcobalt tetrafluoroborate (**1**). A Schlenk flask was charged with cobalt(II) tetrafluoridoborate hexahydrate (0.034 g, 0.100 mmol, 1 equiv) and THF (3 mL) followed by the addition of 1,2-bis(diphenylphosphino)ethane (0.080 g, 0.200 mmol, 2 equiv). The argon atmosphere was then replaced by nitric oxide and the reaction mixture stirred for 1.5 hours, during which the yellow precipitate that had formed upon addition of the diphosphane turned brown. The solvent was filtered off, washed with Et_2O (3× 15 mL) and dried in air for 5 minutes. The bulk product (0.025 g, 0.024 mmol) was filled in a Schlenk flask and acetone was added until the solid was completely dissolved. The solution (2 mL) was transferred to a two-chambered Schlenk flask filled with DMSO (6 mL) in the second chamber in order to force slow evaporation of the solvent. After three days, brown single crystals of **1** suitable for X-ray diffraction were collected. Yield (bulk): 24%. CHN calcd. for $C_{52}H_{48}B_2CoF_8NOP_4$: C, 58.96; H, 4.57; N, 1.32. Found: C, 57.39 (note the 'phosphorus error'); H, 4.55; N, 1.51.

***trans*-Bis(*N*,*N*-dimethylethylenediamine)perchloratonitrosylcobalt perchlorate** (**2**). In a Schlenk flask, a solution of cobalt(II) perchlorate (0.110 g, 0.300 mmol, 1 equiv) in acetone (1.2 mL) was prepared followed by the addition of *N*,*N*-dimethylethylenediamine (0.066 mL, 0.600 mmol, 2 equiv). Then, the argon atmosphere was replaced by nitric oxide. The resulting dark red solution was stirred for 15 minutes. The reaction mixture was transferred to a two-chambered Schlenk flask filled with DMSO (6 mL) in the second chamber. After three days, brown single crystals of **2** suitable for X-ray diffraction were collected (0.013 g, 0.028 mmol). Yield: 9%. CHN calcd. for $C_8H_{24}Cl_2CoN_5O_9$: C, 20.70; H, 5.21; N, 15.09. Found: C, 20.41; H, 5.07; N, 14.99.

Dichlorido-1,2-bis(diphenylphosphino)ethanenitrosylcobalt (**3**). A Schlenk flask was charged with cobalt(II) chloride hexahydrate (0.012 g, 0.050 mmol, 1 equiv) and acetone (1.5 mL) followed by the addition of 1,2-bis-(diphenylphosphino)ethane (0.020 g, 0.050 mmol, 1 equiv). The argon atmosphere was then replaced by nitric oxide and the reaction mixture stirred for 5 minutes. The solution (1.5 mL) was then transferred to a two-chambered Schlenk flask filled with DMSO (5.5 mL) in the second chamber. After two days, brown single crystals of **3** suitable for X-ray diffraction were collected (0.016 g, 0.029 mmol). Yield: 57%. CHN calcd. for $C_{26}H_{24}Cl_2CoNOP_2$: C, 55.94; H, 4.33; N, 2.51. Found: C, 55.11; H, 4.13; N, 2.42.

X-ray analyses

Single crystals of sufficient quality for X-ray diffraction were selected using a Leica MZ6 polarization microscope and measured on a Bruker D8 VENTURE single-crystal diffractometer (APEX3 software) equipped with a Bruker AXS area detector using Mo–Kα radiation (λ = 0.71073 Å) from a Bruker TXS rotating anode. A multiscan absorption correction was applied by using SADABS.[21] The structures were solved by direct methods (SHELXT) and refined by full-matrix least-squares calculations on F^2 (SHELX supported by ShelXle).[22] Thermal ellipsoids were plotted with ORTEP3.[23]

Computational Studies

Structure optimizations and analytical frequency analyses of all species were performed by ORCA, versions 4.2.1 to 5.0.2,[24] using the Karlsruhe Def2 basis sets,[25] their auxiliary basis Def2/J,[26] the density functional BP86,[27] the Becke-Johnson-damped D3 dispersion correction,[28] the implicit solvation model CPCM,[29] and the integration acceleration method RI.[30]

The GGA functional BP86 performs well for geometry optimizations in 3d transition metal systems – even compared to other, more sophisticated choices like GGA hybrid (e.g. B3LYP), meta-GGA hybrid (e.g. TPSSh), or range-separated hybrid (e.g. ωB97X) functionals, which performed just as well as (or worse than) BP86 for our systems.[31] CPCM(∞) was used in all species to simulate the crystal environment, accounting for the prevalent electrostatic interactions and hydrogen bonds which are found even in crystals of electroneutral species. CPCM was not used for the $Q^+\cdots X–Y$ angle scans.

Tables S4–S6 in the Supporting Information show the agreement between the experimental and the computed parameters for the Co–N as well as the N–O distance, the Co–N–O angle, and the energy of the N–O stretch.

Local-mode analysis was performed by LModeA 2.0.0 after adaption of the input routine to the format of ORCA 4/5 hessians.[32]

QTAIM analyses were performed using MultiWFN 3.8.[33] The converged wave functions of the ORCA calculations were converted via orca_2aim from the gbw files to MultiWFN-compatible wfn files in order to prepare atomic-overlap-matrix (aom) files (for QTAIM-derived EOSs) or FCHK files (for TFVC-derived EOSs). Then, the wfn and the aom file was passed to the APOST-3D 4.0 program,[34] together with an input file which specified the fragmentation, yielding the effective fragment orbital (EFO) occupations and finally the oxidation state of each fragment.

Effective oxidation state (EOS) analysis

The background of EOS-related computations in the field of nitrosyl complexes is given in the Experimental Section of Ref. [5], in particular the meaning of the tabulated values for R, λ_{first} and λ_{last}. Table S7 in the Supporting Information contains the result of the EOS analysis. The EOS method itself is introduced and compared with other methods in Refs. [35].

Appendix

Are the {CoNO}^{8} systems of this work adequately described as closed-shell singlets? This question arose in the course of the reviewing process. Since this aspect departs from the common thread of this work, an answer is given in this appendix.

Research Article
doi.org/10.1002/ejic.202200374

Regarding the spin state of {CoNO}^{8} species, singlets are the normal case. However, the significance of triplet states has to be taken into account. Thus, a thermal singlet/triplet equilibrium has been reported for a species which is related to **3**, the bis(phosphane) complex $[CoCl_2(NO)(PMePh_2)_2]$.[36] If reliable experimental structural data are available, the singlet/triplet decision can be based on the marked structural differences of the two states (Ref.[5] shows a worked-out example). Regarding this criterion, all species of this work are safely singlets. Depending on the employed computational methods, both closed-shell and biradical singlets have been reported for {CoNO}^{8} species. In 2015, Radoń has provided an in-depth analysis of the various computational approaches including the background of various DFT functionals' behavior.[37] The origin of the variability of the results is the pronounced static (non-dynamical, left-right) correlation within a Co–NO bond. Figure 7 shows an analysis in terms of a CASSCF(8,7) calculation (8 electrons in 7 orbitals, namely the eigth "Enemark-Feltham electrons" in the five Co-d and the two N–O-π* orbitals) of the $[Co(N,N\text{-dmen})_2(NO)](ClO_4)^+$ part of **2**. From the σ-bond, ca. 1/4 electron is shifted to the respective antibond (MO 96), corresponding to a partial dissociation of the bond. The physical reason is Pauli repulsion on filling an initially empty N–O antibond with a cobalt electron pair. As an NO-π* antibond, there is a respective filled NO-π bond which partly shares the same spatial region with its antibond and thus exerts Pauli repulsion to the approaching electron pair of the metal donor.

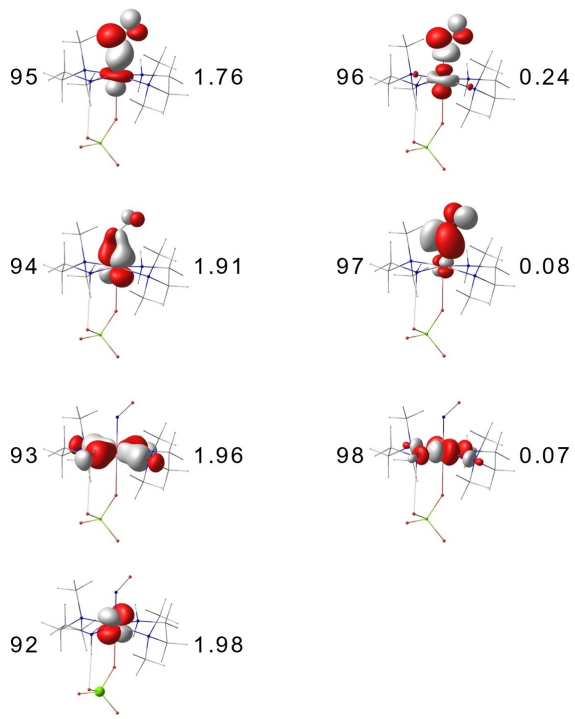

Figure 7. The MOs of the active space of a CASSCF(8,7) calculation on the $[Co(N,N\text{-dmen})_2(NO)](ClO_4)^+$ part of **2** (isovalue 0.06), showing three bond-antibond couples; the two top couples resemble the Co–NO σ- and π-interaction. The MO number mirrors the energetic order; the number right of a contour is the occupation of the respective MO with electrons. The Co–NO σ-bond (MO 95) as well as the π-bond (MO 94) show the largest deviation from the 2222000 configuration (which contributes with 84% weight to the wave function).

In a DFT framework, the trace of static correlation depends on the type of the employed functional. Non-hybrid functionals such as the GGA functional BP86 used in this work or the meta-GGA functional TPSS tend to underestimate the bond-lengthening effect visible in the CASSCF MOs but show this behavior both in closed-shell as well as in broken-symmetry approaches. Contrarily, hybrid functionals such as TPSSh (10% HF exchange) or B3LYP (20% HF exchange) tend to singlet biradical solutions for the Co–NO bond in the course of a broken-symmetry (BS) treatment. The computational background of the behavior that static correlation manifests itself as a singlet-biradical state in broken-symmetry DFT approaches using hybrid functionals is clarified in the above-mentioned work by Radoń.[37]

For the ground states of **1**, **2** and **3**, as well as for the $[Co(dmpe)_2(NO)]^{2+}$ homologue of the cation of **1** (see the SI), we compared the closed-shell singlet solution and broken-symmetry approaches using the same level of theory (*method*/def2-TZVP + D3 + CPCM(∞) with *method* = BP86, TPSS, TPSSh and B3LYP). The results confirmed the previous experience. For the pure functionals BP86 and TPSS, the broken-symmetry calculation fell back to the closed-shell solution with the energies being the same for all species, with $\langle S^2\rangle_{BS} = 0.000$, and with the overlap of the corresponding orbitals $S_{\alpha\beta}$ being 1.000 (all calculations with Orca 5.0.3; for the corresponding-orbital concept see Ref.[38]). For the hybrid functionals TPSSh and B3LYP, broken-symmetry solutions were obtained for **2** and **3**, whereas the broken-symmetry computation fell back to the closed-shell singlet for the linear-type species **1** and its $[Co(dmpe)_2(NO)]^{2+}$ homologue.

Table 3 shows the results for the $[Co(N,N\text{-dmen})_2(NO)](ClO_4)^+$ part of **2** in its bent GS. Typically, the Co–N distances are too short for the pure functionals. At the same time, the N–O stretch is reproduced best (which is a major reason to use BP86 as the standard method in this work). For the hybrid functionals, the broken-symmetry solution was more stable than the closed shell result, 0.7 kJ mol^{-1} for TPSSh, 12.9 kJ mol^{-1} for B3LYP. TPSSh gave a better Co–N distance, broken-symmetry-TPSSh was still better. As not unusual in nitrosyl chemistry, B3LYP performed worse in terms of the N–O stretch. Broken-symmetry-B3LYP showed marked biradicaloid character but led to unacceptable values for the Co–N distance and the N–O stretch.

Table 3. The $[Co(N,N\text{-dmen})_2(NO)](ClO_4)^+$ part of **2** in various *method*/def2-TZVP + D3 + CPCM approaches (Orca keywords for the CPCM correction: surface type gepol_sas, $r_{solv} = 0.6$).

	Co–N/Å	N–O/Å	Co–N–O/°	$\tilde{\nu}_{NO}$/cm^{-1}
Exp.	1.809(2)	1.165(2)	123.6(2)	1655
BP86/$BP86_{BS}$	1.779	1.185	122.9	1637
TPSS/$TPSS_{BS}$	1.788	1.186	122.1	1637
TPSSh	1.793	1.176	121.0	1693
$TPSSh_{BS}$[a]	1.815	1.173	121.9	1703
B3LYP	1.821	1.166	120.3	1737
$B3LYP_{BS}$[b]	1.935	1.154	124.1	1822

[a] $S_{\alpha\beta} = 0.914$, $\langle S^2\rangle_{BS} = 0.172$; [b] $S_{\alpha\beta} = 0.650$, $\langle S^2\rangle_{BS} = 0.595$.

Research Article
doi.org/10.1002/ejic.202200374

The same approach was applied to the ground state of **3**. Again, for BP86 and TPSS, the broken-symmetry solution fell back to the closed-shell singlet. For the hybrid functionals, the broken-symmetry solution was more stable than the closed shell result, 1.0 kJ mol^{-1} for TPSSh, 14.8 kJ mol^{-1} for B3LYP. Table 4 shows the results which mirror all the details described above for the case of **2** including the gross errors produced by broken-symmetry-B3LYP. (For this neutral molecule, there is less justification to apply a CPCM correction. However, it was applied for the sake of uniformity. See the table caption for a comparison of BP86 and B3LYP approaches without the CPCM correction.)

In summary, the known rules apply to the species of this work. However, have the various approaches an effect upon the key numbers of this work, the linear/bent charge differences and the bond-strength measures? Table 5 collects such data for **2** and its unstable tentative isomer **2′** by comparing TPSSh and broken-symmetry-TPSSh computations. TPSSh was chosen (instead of B3LYP) due to the satisfactory match of computed and experimental data.

The first data block summarizes the key data for this work. Starting with the QTAIM charge Q/e of the nitrosyl ligand, the broken-symmetry values show a difference of 0.03 between **2** (−0.24) and **2′** (−0.21), the respective values of Table 2 of **2** (−0.27) and **2′** (−0.24) exhibiting the same difference. The next item, the Co–N and N–O force constants show the non-DCD behavior of the linear/bent transition in both tables. A closer look at the local force constant of the Co–N bond shows a notably weaker bond of the bent species in the broken-symmetry computation compared with the closed-shell-TPSSh numbers.

The second data block collects various numbers which characterize the broken-symmetry state (the corresponding-orbital overlap $S_{\alpha\beta}$, the $\langle S^2\rangle$ value, and the relative energy). The third block is devoted to a secondary issue of this work, oxidation states. These are collected in Table S7 in the SI. **1**–**3**, as well as about 20 {CoNO}^{8} species of Ref. [5] show R values close to 50% on EOS determination. The values mirror a characteristic property of Co–NO bonds, their covalency. The borderline character of the EOS values causes some degree of method dependency as has been exemplified in Ref. [5]. Thus, most methods result, in a borderline manner, in $EOS_{NO} = +1$, including the parameters from the CASSCF(8,7) computation on **2**: $Q_{NO}/e = -0.193$, $EOS_{NO} = +1$, $R = 51.6\%$. The only exception is the broken-symmetry-TPSSh computation on the bent ground state of **2**. Here, the α/β separation of the broken-symmetry treatment is conserved by the EOS method and results in the assignment of the α-spin to the metal and the β-spin to the nitrosyl ligand. The thus homolytic cleavage of the largely covalent bond results in a high R value which, of course, makes sense from a computational perspective. However, we end up with a conceptual problem. Homolytic cleavage of a bond between different elements is not part of the current oxidation-state concepts, be this bond covalent as it may.

To answer the initial question, we can state that the well-known challenges of nitrosyl-metal bonding are present also for the new species of this work. However, the computational intricacies do not touch the focus of this work, the spectroscopic consequences of the non-DCD behavior of bending a linear nitrosyl-metal moiety.

Table 4. **3**; *method*/def2-TZVP + D3 + CPCM. Values without the CPCM correction in the same order as the table entries: BP86 1.717 Å, 1.179 Å, 141.1°, 1684 cm^{-1}; B3LYP 1.736 Å, 1.164 Å, 134.5°, 1741 cm^{-1}.

	Co–N/Å	N–O/Å	Co–N–O/°	$\tilde{\nu}_{NO}$/cm^{-1}
exp.	1.750(1)	1.173(2)	137.9(1)	1667
BP86/BP86$_{BS}$	1.719	1.177	140.9	1666
TPSS/TPSS$_{BS}$	1.721	1.174	141.0	1674
TPSSh	1.717	1.166	138.1	1716
TPSSh$_{BS}$[a]	1.747	1.166	137.7	1722
B3LYP	1.742	1.161	132.4	1725
B3LYP$_{BS}$[b]	1.859	1.157	134.0	1774

[a] $S_{\alpha\beta} = 0.900$, $\langle S^2\rangle_{BS} = 0.218$; [b] $S_{\alpha\beta} = 0.774$, $\langle S^2\rangle_{BS} = 0.479$.

Table 5. Closed-shell *versus* broken-symmetry singlets. TPSSh/def2-TZVP + D3 + CPCM calculation of the $[Co(N,N\text{-dmen})_2(NO)](ClO_4)^+$ part of **2** including the unstable linear isomer **2′**.

	2			**2′**	
	Exp.	TPSSh	BS-TPSSh	TPSSh	BS-TPSSh
Co–N/Å	1.809(2)	1.793	1.815	1.650	1.651
N–O/Å	1.165(2)	1.176	1.173	1.150	1.150
Co–N–O/°	123.6(2)	121.0	121.9	177.4	178.2
$\tilde{\nu}_{NO}$/cm^{-1}	1655	1693	1703	1897	1896
Q_{NO}/e		−0.26	−0.24	−0.21	−0.21
$k^a_{Co\text{-}N}$/N cm^{-1}		2.192	1.414	4.030	4.043
$k^a_{N\text{-}O}$/N cm^{-1}		12.176	12.115	14.808	14.737
$S_{\alpha\beta}$(HOMO)			0.914		0.982
$S_{\alpha\beta}$(HOMO−1)			0.998		0.985
$\langle S^2\rangle_{BS}$			0.172		0.068
E_{rel}/kJ mol^{-1}		0.7	0	42.9	43.0
EOS_{NO}		+1	0	+1	+1
R		52.5	80.2	57.1	57.0

Supporting Information

See footnote on the first page of this article: Details of the X-ray analyses (Tables S1–S4), experimental vs. computed values for the species of Tables 1 and 2 (Tables S4–S6). Details of the effective-oxidation-state calculations including an example of an effective-fragment-orbital partitioning (Figure S1 and Table S7), additional angle scans on $^3NO^-$ (Figure S2) and singlet-diazenide (Figure S3), including a comment on the origin of the tabulated experimental fundamentals of CO and NO. Additional charges from various methods for the entries of Tables 1 and 2 of the main text. A Badger plot for the carbonyls of Table 1 (Figure S4); *xyz* lists for all computed species, a chapter on the significance of the steric bulk of phenylphosphino moieties, and a chapter on the effect of varying the magnitude of the probe charge.

Deposition Numbers 2129959 (for **1**), 2129960 (for **2**), and 2129961 (for **3**) contain the supplementary crystallographic data for this paper. These data are provided free of charge by the joint Cambridge Crystallographic Data Centre and Fachin-

formationszentrum Karlsruhe Access Structures service www.ccdc.cam.ac.uk/structures.

Acknowledgements

*We gratefully acknowledge financial support from the DFG priority program SPP1740 (KL 624/18-1), aimed at "Reactive bubbly flows". Daniel Schröder is acknowledged for his support in the computations on **1**. We are indebted to Pedro Salvador for helpful discussions. Open Access funding enabled and organized by Projekt DEAL.*

Conflict of Interest

The authors declare no conflict of interest.

Data Availability Statement

The data that support the findings of this study are available in the supplementary material of this article.

Keywords: Acceptor ligands · Backbonds · Local-mode analysis · Nitrosyl ligands · Oxidation state

[1] A. Haaland, *Angew. Chem. Int. Ed. Engl.* **1989**, *28*, 992–1007.
[2] a) E. Kraka, W. Zou, Y. Tao, *WIREs Comput. Mol. Sci.* **2020**, *10*, e1480; b) L. Zhao, M. Zhi, G. Frenking, *Int. J. Quantum Chem.* **2021**, e26773.
[3] J. H. Enemark, R. D. Feltham, *Coord. Chem. Rev.* **1974**, *13*, 339–406.
[4] E. Ramos-Cordoba, P. Salvador, I. Mayer, *J. Chem. Phys.* **2013**, *138*, 214107.
[5] J. Popp, T. Riggenmann, D. Schröder, T. Ampßler, P. Salvador, P. Klüfers, *Inorg. Chem.* **2021**, *60*, 15980–15996.
[6] R. D. Feltham, R. S. Nyholm, *Inorg. Chem.* **1965**, *4*, 1334–1339.
[7] a) J. H. Enemark, R. D. Feltham, *PNAS* **1972**, *69*, 3534; b) J. H. Enemark, R. D. Feltham, *J. Am. Chem. Soc.* **1974**, *96*, 5004–5005; c) J. H. Enemark, R. D. Feltham, *J. Am. Chem. Soc.* **1974**, *96*, 5002–5004; d) J. H. Enemark, R. D. Feltham, J. Riker-Nappier, K. F. Bizot, *Inorg. Chem.* **1975**, *14*, 624–632; e) J. H. Enemark, R. D. Feltham, B. T. Huie, P. L. Johnson, K. B. Swedo, *J. Am. Chem. Soc.* **1977**, *99*, 3285–3292.
[8] a) M. E. Jacox, W. E. Thompson, *J. Chem. Phys.* **1990**, *93*, 7609–7621; b) K. K. Irikura, *J. Phys. Chem. Ref. Data* **2007**, *36*, 389–397.
[9] a) A. S. Goldman, K. Krogh-Jespersen, *J. Am. Chem. Soc.* **1996**, *118*, 12159–12166; b) A. J. Lupinetti, S. Fau, G. Frenking, S. H. Strauss, *J. Phys. Chem. A* **1997**, *101*, 9551–9559.
[10] R. Kalescky, E. Kraka, D. Cremer, *J. Phys. Chem. A* **2013**, *117*, 8981–8995.
[11] L. E. Hatcher, P. R. Raithby, *Acta Crystallogr. Sect. C* **2013**, *69*, 1448–1456.
[12] a) T. E. Bitterwolf, *Coord. Chem. Rev.* **2006**, *250*, 1196–1207; b) P. Coppens, I. Novozhilova, A. Kovalevsky, *Chem. Rev.* **2002**, *102*, 861–884; c) P. Gütlich, Y. Garcia, T. Woike, *Coord. Chem. Rev.* **2001**, *219–221*, 839–879.
[13] K. R. Sawyer, R. P. Steele, E. A. Glascoe, J. F. Cahoon, J. P. Schlegel, M. Head-Gordon, C. B. Harris, *J. Phys. Chem. A* **2008**, *112*, 8505–8514.
[14] A. Zangl, P. Klüfers, D. Schaniel, T. Woike, *Dalton Trans.* **2009**, 1034–1045.
[15] S. F. McWilliams, P. L. Holland, *Acc. Chem. Res.* **2015**, *48*, 2059–2065.
[16] A. Brinkmeier, K. E. Dalle, L. D'Amore, R. A. Schulz, S. Dechert, S. Demeshko, M. Swart, F. Meyer, *J. Am. Chem. Soc.* **2021**, *143*, 17751–17760.
[17] a) J. F. Van der Maelen, *Organometallics* **2020**, *39*, 3458–3460; b) J. F. Van der Maelen, *Organometallics* **2020**, *39*, 132–141; c) N. Holzmann, I. Fernández, G. Frenking, *Organometallics* **2020**, *39*, 2956–2958.
[18] S. Fernández-Moyano, M. N. Peñas-Defrutos, C. Bartolomé, P. Espinet, *Inorg. Chem.* **2021**, *60*, 14410–14417.
[19] J. Cioslowski, G. Liu, R. A. Mosquera Castro, *Chem. Phys. Lett.* **2000**, *331*, 497–501.
[20] Q. Wang, S. H. Brooks, T. Liu, N. C. Tomson, *Chem. Commun.* **2021**, *57*, 2839–2853.
[21] L. Krause, R. Herbst-Irmer, G. M. Sheldrick, D. Stalke, *J. Appl. Crystallogr.* **2015**, *48*, 3–10.
[22] a) G. Sheldrick, *Acta Crystallogr. Sect. C* **2015**, *71*, 3–8; b) G. M. Sheldrick, *Acta Crystallogr. Sect. A* **2015**, *71*, 3–8; c) C. B. Hübschle, G. M. Sheldrick, B. Dittrich, *J. Appl. Crystallogr.* **2011**, *44*, 1281–1284.
[23] L. Farrugia, *J. Appl. Crystallogr.* **2012**, *45*, 849–854.
[24] a) F. Neese, *WIREs Comput. Mol. Sci.* **2018**, *8*, e1327; b) F. Neese, *WIREs Comput. Mol. Sci.* **2012**, *2*, 73–78.
[25] F. Weigend, R. Ahlrichs, *Phys. Chem. Chem. Phys.* **2005**, *7*, 3297–3305.
[26] F. Weigend, *Phys. Chem. Chem. Phys.* **2006**, *8*, 1057–1065.
[27] a) A. D. Becke, *Phys. Rev. A* **1988**, *38*, 3098–3100; b) J. P. Perdew, *Phys. Rev. B* **1986**, *33*, 8822–8824.
[28] a) S. Grimme, J. Antony, S. Ehrlich, H. Krieg, *J. Chem. Phys.* **2010**, *132*, 154104; b) S. Grimme, S. Ehrlich, L. Goerigk, *J. Comput. Chem.* **2011**, *32*, 1456–1465.
[29] V. Barone, M. Cossi, *J. Phys. Chem. A* **1998**, *102*, 1995–2001.
[30] F. Neese, F. Wennmohs, A. Hansen, U. Becker, *Chem. Phys.* **2009**, *356*, 98–109.
[31] a) K. P. Jensen, B. O. Roos, U. Ryde, *J. Chem. Phys.* **2007**, *126*, 014103; b) J. N. Harvey, *Annu. Rep. Prog. Chem., Sect. C: Phys. Chem.* **2006**, *102*, 203–226.
[32] W. Zou, Y. Tao, M. Freindorf, M. Makos, N. Verma, E. Kraka, *Dallas* **2020**.
[33] T. Lu, F. Chen, *J. Comput. Chem.* **2012**, *33*, 580–592.
[34] P. Salvador, E. Ramos-Cordoba, M. Gimferrer, M. Montilla, *Universitat de Girona, Spain* **2010**.
[35] a) E. Ramos-Cordoba, V. Postils, P. Salvador, *J. Chem. Theory Comput.* **2015**, *11*, 1501–1508; b) V. Postils, C. Delgado-Alonso, J. M. Luis, P. Salvador, *Angew. Chem. Int. Ed.* **2018**, *57*, 10525–10529; *Angew. Chem.* **2018**, *130*, 10685–10689; c) M. Gimferrer, J. Van der Mynsbrugge, A. T. Bell, P. Salvador, M. Head-Gordon, *Inorg. Chem.* **2020**, *59*, 15410–15420.
[36] H. J. B. Marroux, B. F. E. Curchod, C. A. Faradji, T. A. Shuttleworth, H. A. Sparkes, P. G. Pringle, A. J. Orr-Ewing, *Angew. Chem. Int. Ed.* **2017**, *56*, 13713–13716; *Angew. Chem.* **2017**, *129*, 13901–13904.
[37] M. Radoń, *Inorg. Chem.* **2015**, *54*, 5634–5645.
[38] F. Neese, *J. Phys. Chem. Solids* **2004**, *65*, 781–785.

Manuscript received: June 9, 2022
Revised manuscript received: August 10, 2022
Accepted manuscript online: August 26, 2022